



# Numerical investigation of gas migration behaviour in saturated bentonite with consideration of temperature

Lin-Yong Cui<sup>1,2</sup> · Shakil A. Masum<sup>2</sup> · Wei-Min Ye<sup>1</sup> · Hywel R. Thomas<sup>2</sup> · Chao Zhou<sup>3</sup> · Hong-Qiang Hu<sup>4</sup>

Received: 7 June 2022 / Accepted: 15 January 2024  
© The Author(s) 2024

## Abstract

Gas migration behaviour in saturated, compacted bentonite, especially under rigid-boundary conditions, is controversial. Gas breakthrough phenomena, observed under higher pressure gradient conditions in laboratory experiments, are described in literatures by adopting visco-capillary or dilatancy-controlled flow concept. Since, under rigid-boundary conditions, volumetric expansion is restricted and/or water dissipation is not detected, these concepts cannot be implemented satisfactorily. Instead, a diffusion and solubility-controlled (DSC) flow concept was previously found to be adequate for describing the behaviours at lower temperatures (20 °C). The DSC concept describes gas breakthrough as a function of gas solubility. Breakthrough occurs when concentration of dissolved gas reaches or surpasses the solubility limit in the entire specimen. In this work, the DSC flow concept is applied to validate gas migration and breakthrough experiments conducted at higher temperatures, e.g. 40 and 60 °C. Good agreements are observed between the experimental and predicted results, suggesting that the DSC flow concept can be applied to describe gas migration behaviour satisfactorily in rigidly confined saturated bentonites (under constant volume conditions) for various temperature regimes. Results also show that helium dissolution and diffusion processes in saturated bentonite are sensitive to test temperature and pressure conditions. The processes become more stable with increasing gas injection pressure and ambient temperature.

**Keywords** Diffusion · Gas breakthrough · GMZ bentonite · Simulation · Solubility · Temperature

## 1 Introduction

Deep geological disposal of high-level radioactive waste materials is a widely accepted strategy to ensure safety and containment of radionuclides in subsurface environment for long, geological period of time. The strategy is based on a multi-barrier system where radioactive waste canisters

are surrounded by pure bentonite or bentonite-based clay materials, also known as engineered barriers. The bentonite barriers encapsulate waste canisters in host rock deposits and provide major containment or buffering against radionuclide migration. Its high swelling property, low permeability, high sorption capacity and good self-sealing characteristics [5, 10, 23, 27, 28, 43] make it an ideal buffer material. Safety and structural integrity of a repository largely depends on the performance of bentonite barriers [33]. Existing investigations revealed that repository gases resulted from corrosion of metallic waste canisters, radiolysis of water or degradation of organic materials [7, 8, 14, 21, 26, 40] could led to gas generation and migration-related risks or failure of the barrier system.

Gas migration in bentonite, especially when saturated and subjected to rigid-boundary conditions, is contentious. Four mechanisms are reported in literatures including diffusion and solubility-controlled transport, visco-capillary flow, dilatancy-controlled flow and gas migration through macro-fracture [24, 42]. Two-phase, visco-capillary flow

---

✉ Shakil A. Masum  
MasumSA1@cardiff.ac.uk

<sup>1</sup> Department of Geotechnical Engineering, College of Civil Engineering, Tongji University, Shanghai 200092, China

<sup>2</sup> Geoenvironmental Research Centre, Cardiff School of Engineering, Cardiff University, Queen's Buildings, The Parade, Cardiff CF24 3AA, UK

<sup>3</sup> Department of Civil and Environmental Engineering, The Hong Kong Polytechnic University, Hung Hom, Hong Kong

<sup>4</sup> School of Civil Engineering and Architecture, Zhejiang University of Science and Technology, Hangzhou 310023, China

[12, 13] in bentonite under the stated condition is rarely observed in the experimental investigations. This is because water in bentonite pores, under high ionic strength environment, forms a viscous ‘clay-gel’-like substance, rather than existing as typical porewater, which would require extremely high gas pressure to activate pressure-induced visco-capillary flow. Meanwhile, dilatancy-controlled [16–18] or macro-fractures flow [23] would require volume expansion or gas pressure exceeding the sum of minimum principal stress and tensile strength of the medium. Although such mechanism may occur under flexible or semi-rigid conditions, they cannot explain the behaviour under constant volume or fixed boundary condition. These mechanisms assume that diffusive gas transport would not discharge generated gases adequately from the canister–buffer interface causing development of excessive gas pressures at the interface. Limited attempts are made to test the hypothesis both in laboratory investigations and in numerical modelling studies.

In recent studies, Cui et al. [6] conducted a series of gas migration and breakthrough experiments on GMZ bentonites and analysed the results by employing a novel diffusion and solubility-controlled (DSC) flow concept [4]. The concept was developed and implemented under a coupled reactive gas transport model [25, 34]. The aim of the study [4] was to investigate the extent to which diffusion and solubility driven flow could explain gas migration behaviours in saturated, rigidly confined bentonites. From the detailed analysis, it was found that DSC can be used to describe gas flow and breakthrough behaviour in GMZ bentonites satisfactorily. However, only the results of the experiments, conducted at the 20 °C, were assessed and validated. The question remained whether the DSC flow concept could describe the migration and breakthrough phenomena at higher temperatures. Temperature has significant impact on fluid properties including surface tension, contact angle, viscosity and boundary layers of porewater [2, 11, 41, 44], which may eventually lead to different gas migration behaviours. Therefore, repository design and safety assessment processes require comprehensive understanding of gas migration and breakthrough behaviours at elevated temperature regimes.

Temperature effects on saturated clays have been investigated in laboratory investigations [3, 6, 9, 29, 31] and, generally, it was observed that gas breakthrough pressure decreased with temperature. Cui et al. [6] attributed this phenomenon to reduce liquid surface tension and increase of cross-sectional area of flow pathways, allowing easier water displacement through bentonite specimens. However, no direct water displacement was observed, and the hypothesis was tested by measuring water contents before and after the experiments which was found lower after the tests. Loss of moisture perhaps might be due to

evaporation or consolidation rather than actual displacement. More studies are required to improve understanding and scientific knowledgebase of gas migration and breakthrough behaviour of GMZ bentonites. The material is being considered as a candidate material for nuclear waste repositories in China [35]. In this work, temperature effects on gas transport and breakthrough behaviours of compacted saturated GMZ bentonites, subjected to fixed boundary conditions, are examined. Cui et al. [6] conducted gas breakthrough experiments on GMZ bentonite samples of 1.5 g/cm<sup>3</sup> dry density at 20, 40 and 60 °C. Helium gas was injected in water-saturated specimens using the residual capillary pressure (RCP) method. In this paper, the experimental results are analysed using the diffusion and solubility-controlled flow concept proposed in Cui et al. [4]. The aim is to test and assess validity of the concept for describing the observed gas transport phenomena at higher temperatures. In the following sections, we briefly present: (i) the experimental procedures; (ii) the theoretical background; (iii) the simulation set-ups; and (iv) finally, a comprehensive discussion and analysis of the results.

## 2 Experimental procedures

### 2.1 Materials and methods

The bentonite samples, GMZ01, were extracted from the GaoMiaoZi county in the Inner Mongolia Autonomous Region, 300 km northwest from Beijing, China. The GMZ01 bentonite used in this work is a light grey powder, dominated by montmorillonite. The basic properties of the

**Table 1** Basic physical and chemical properties of GMZ bentonite [35]

Properties	Description
Specific gravity of soil grain	2.66
pH	8.68–9.86
Liquid limit (%)	276
Plastic limit (%)	37
Total specific surface area (m <sup>2</sup> /g)	597
Cation exchange capacity (mmol/100 g)	77.3
Main exchanged cation (mmol/100 g)	Na <sup>+</sup> (43.36), Ca <sup>2+</sup> (29.14), Mg <sup>2+</sup> (12.33), K <sup>+</sup> (2.51)
Main minerals	Montmorillonite (75.4%), quartz (11.7%), feldspar (4.3%), cristobalite (7.3%)

GMZ01 bentonite are presented in Table 1 [35]. The material exhibits high cation exchange capacity, and alkaline in nature.

For sample preparation, bentonite powder of 10.7% initial water content was statically compacted at a speed of 0.3 mm/min to a target dry density of 1.5 g/cm<sup>3</sup>. Compaction was stopped when the cylindrical specimens of 50.15 mm diameter reached to 10.21 mm height.

## 2.2 Apparatus and test procedures

The residual capillary pressure (RCP) approach [1, 20, 39] was employed to conduct the gas injection tests on water-saturated bentonite specimens under different temperature conditions. Experimental apparatus and schematic diagram of the gas injection tests are presented in Fig. 1.

Prior to the gas injection tests, the specimen temperature was controlled at 20 °C by a digital oven with an accuracy of ± 0.1 °C. Then the specimen was saturated with deionized water by a liquid volume/pressure controller at injection pressure ( $P_w$ ) of 1 MPa (Fig. 1a). Water infiltration was recorded using the liquid volume/pressure controller. The specimen was considered as fully saturated ( $S_w > 0.99$ ) when a continuous outflow was observed at the bottom of the specimen and the variation of water injection reached to a stabilized state (after about 7–10 days). After that, the liquid volume/pressure controller at the top side of the cell was shifted to connect to the receiving gas compartment while the bottom side of the specimen cell was connected to the gas injection compartment for the subsequent gas injection test (Fig. 1b).

To conduct the gas injection tests using the RCP method, gas pressure in the injection compartment ( $P_1$ ) was then increased to a target value using the booster pump, while in the receiving compartment ( $P_2$ ) atmospheric pressure was maintained. Both compartments were then sealed and the gas injection test was initiated. In this study, inner volume of the injection or receiving compartments was fixed at 100 cm<sup>3</sup>. As the tests were proceeded, gas pressure in the injection compartment gradually decreased while that in the receiving compartment it increased (Fig. 1c). Gas pressure evolution was recorded by gas pressure sensors throughout the tests. Gas injection test on a specimen was stopped either after around 20 days or when a distinct gas breakthrough was observed, which was characterized by the rapid decrease of the pressure difference ( $\Delta P = P_1 - P_2$ ) between the two compartments. Then, the experimental set-up was dismantled, and a new as-prepared bentonite specimen was installed with a higher initial gas injection pressure. The gas injection pressures that were applied, at different temperatures, are listed in Table 2.

Note that temperature calibration was conducted prior to the water and gas injection tests. A linear correlation was observed between the temperature inside the specimen and the set temperature by the digital oven with a 30-min time lag. That relationship was employed to control the specimen temperature during the water and gas injection tests.

## 3 Theoretical background

### 3.1 Temperature-dependent solubility of gases in pore liquid

At a constant temperature, solubility of gases in liquid can be calculated by Henry's law following,

$$u_g = K_{H(T)} \times c_l \quad (1)$$

where  $K_{H(T)}$  is the Henry's constant as a function of temperature (L·atm/mol),  $c_l$  is the concentration of the dissolved gas in liquid (mol/L) and  $u_g$  is the partial pressure of the gas at the gas phase (atm). Henry's constants for helium, at various temperatures, are collected from literature and summarized in Fig. 2. Data fitting exercise yields the following relationship between the constant  $K_{H(T)}$  and temperature  $T$  (°C):

$$K_{H(T)} = -0.17 \times (T - 33.94)^2 + 2587.16 \quad (2)$$

Table 3 shows the values of  $K_{H(T)}$  considered by Cui et al. [6].

It should be noted that, Henry's law might be only validated for the dissolved gas with low concentration (below 3 mol%) and partial pressure, since the relationship between the gas pressure and the concentration of dissolved gas would not be linear under very high-pressure levels. Even though, Wiebe and Gaddy [36] measured the solubility of helium gas in water for a range of atmospheric pressures under different temperatures and their results showed that, at a given temperature, the solubility of helium gas is in a linear relationship with pressure (Fig. 3). Therefore, it was assumed that, Henry's law remains applicable for helium gas within the pressure range studied in this work, approximately 0–5 MPa (Table 2).

Gas solubility in liquid is limited. Only a certain amount can be dissolved until it reaches to the saturation ( $\Omega$ ) with respect to the gas component. Gas dissolution in bentonite porewater is a transient process while  $\Omega < 1.0$ , i.e. under-saturated with respect to the gas. Concentration of dissolved gas in porewater continues to increase until it reaches equilibrium or full saturation, i.e.  $\Omega = 1.0$ . At this stage, gas dissolution rate in the liquid phase is equal to its exsolution rate. When  $\Omega > 1.0$ , the solution is super-

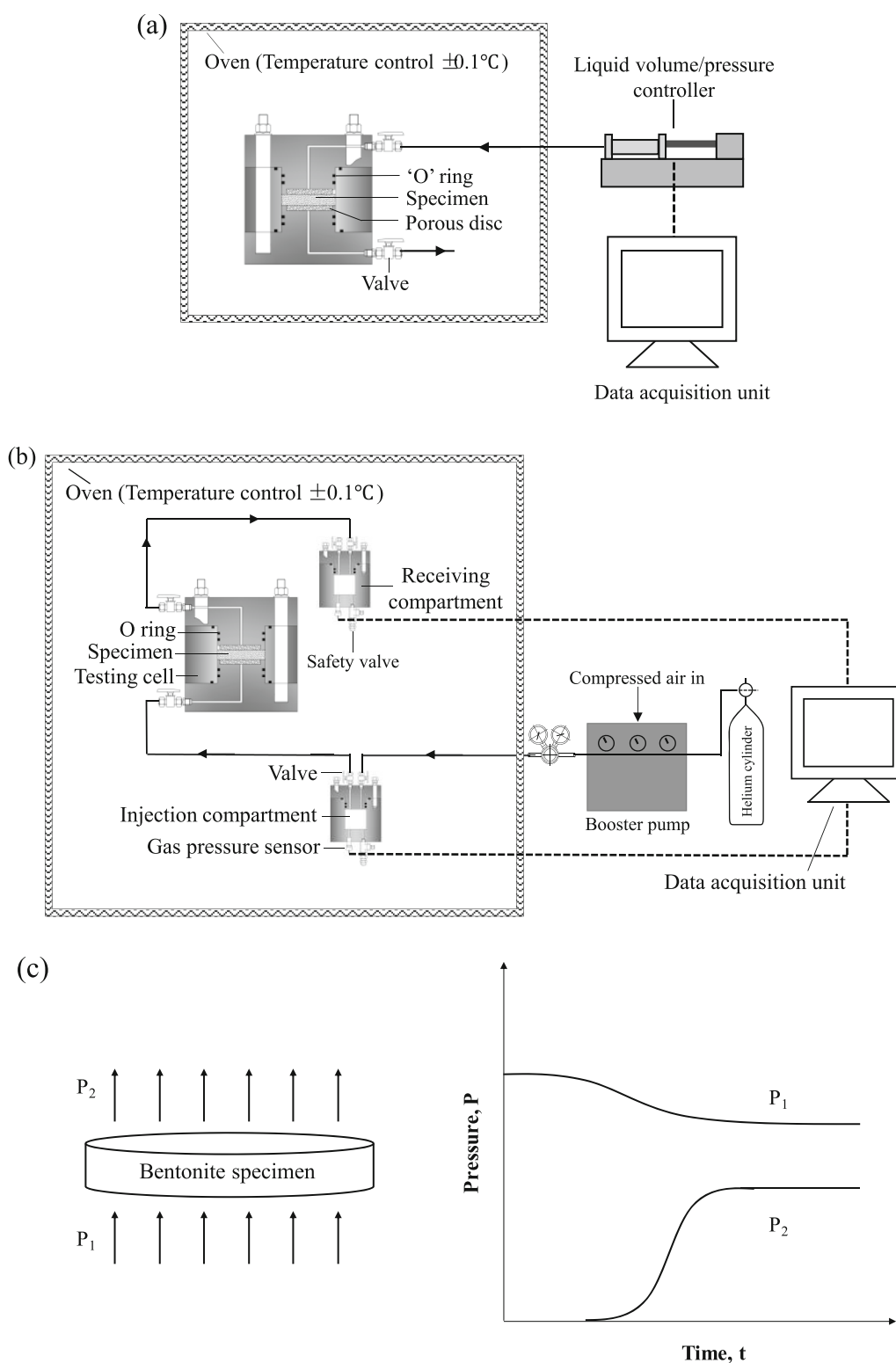


**Fig. 1** Experimental apparatus for hydration of the specimen (a), experimental set-up of gas injection test (b) and schematic diagram for gas injection tests (c) [4]

saturated with respect to the gas and no more gas can be dissolved. Since the system reaches to a steady state, gas dissolution in the porewater should be balanced,

instantaneously, by an equal amount of gas exsolution. When such condition prevails all over the bentonite sample, i.e. the whole sample reaches to a steady state in terms

**Table 2** Specifications of gas breakthrough tests conducted by Cui et al. [6]

Specimen No	Water hydration $P_w$ (MPa)	Helium injection test $P_1$ (MPa)	Controlling temperature (°C)
1	1	2.31	20
2	1	3.12	20
3	1	3.66	20
4	1	4.11	20
5	1	4.31	20
6	1	1.25	40
7	1	2.31	40
8	1	3.15	40
9	1	3.64	40
10	1	3.94	40
11	1	1.25	60
12	1	2.31	60
13	1	2.63	60
14	1	2.92	60

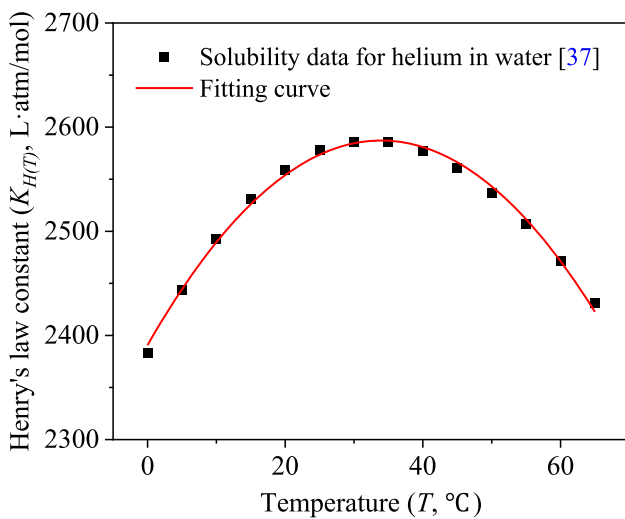


**Fig. 2** Solubility of helium in water for various temperatures [37]

**Table 3** Henry's law constants for helium gas under different temperatures

Temperature (°C)	Henry's law constant (L·atm/mol)
20	2580
40	2585
60	2437

of dissolved gas concentration or the solubility limit ( $c_l = c_{l,max}$ ), gas breakthrough occurs. This phenomenon is

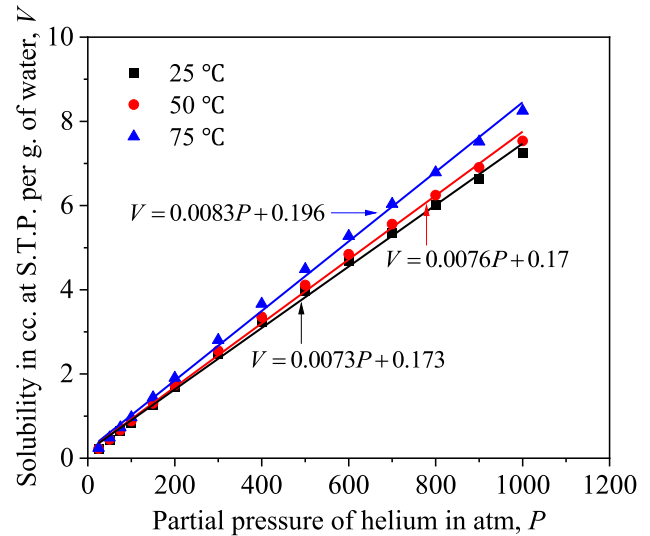


**Fig. 3** Solubility of helium gas in water with varying pressure under different temperatures (data from Wiebe and Gaddy [36])

observed in the laboratory experiments when the outlet gas pressure suddenly rises or inlet gas pressure suddenly drops. No water displacement is required to describe the gas breakthrough phenomenon under solubility-controlled flow mechanism, and it is consistent with the laboratory observations. A graphical representation of the solubility-controlled flow is presented in Fig. 4.

### 3.2 Diffusion of gases in pore liquid

The diffusive mass flux  $F$  (mol/m<sup>2</sup>/s), driven by concentration gradient, is expressed by Fick's first law:

$$F = -D_g \frac{dc}{dx} \tag{3}$$

where  $D_g$  denotes the effective diffusion coefficient in the porous media (m<sup>2</sup>/s) and is defined as:

$$D_g = \eta \times D_a \tag{4}$$

where  $D_a$  is the apparent diffusion coefficient (m<sup>2</sup>/s) and  $\eta$

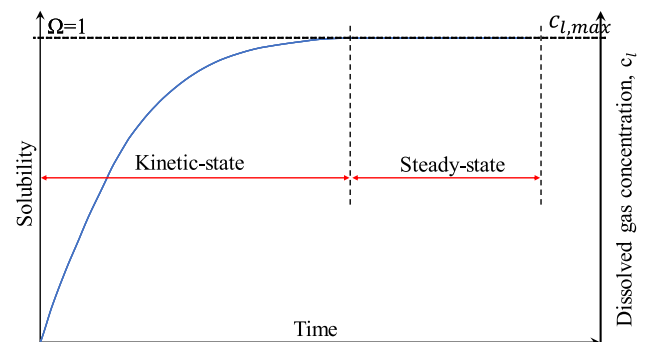


**Fig. 4** Graphical representation of the solubility-controlled gas breakthrough in bentonite [4]

is the effective transport-through porosity which could account for the cross-sectional area available for diffusion when diffusion occurs only in pore space [15]. In this study, the value of  $\eta$  is considered same as the porosity of the specimen. Higashihara et al. [19] and Sato et al. [32] considered path geometry and viscosity of bentonite porewater in their experiments. Since retardation of helium due to adsorption is negligible, the apparent diffusion coefficient of helium in saturated compacted montmorillonite is described as,

$$D_a = \left( \frac{\delta}{\tau_l^2} \right) \times D_{b(T)} \quad (5)$$

where  $D_{b(T)}$  is the temperature-dependent diffusion coefficient ( $\text{m}^2/\text{s}$ ) of dissolved chemicals or gases in bulk water. Wise and Houghton [38] estimated the bulk diffusion of helium in water as a function of temperature (Fig. 5a). The ratio  $\delta/\tau_l^2$  is known as formation factor that accounts for the diffusive path being filled with the modified water instead of just porewater, which is closely related to the dry density [32] of a specimen. Sato et al. [32] reported the formation factor of Na-montmorillonite, as a function of its dry densities, which are presented in Fig. 5b. Finally, the apparent diffusion coefficient for compacted bentonite at different temperatures could be determined and its values are listed in Table 4.

### 3.3 Governing equations

The aforementioned equations are included the governing poregas transport equation:

$$\frac{\partial(\theta_k c_k)}{\partial t} = \nabla(D_k \nabla c_k) + \nabla(u_k c_k) \pm s_k \quad k \in \{l, g\} \quad (6)$$

where  $c_k$  represents concentration of gas in gas phase ( $c_g$ ) or in the liquid phase ( $c_l$ ) as dissolved or aqueous state.  $D_k$  is the effective diffusion coefficient and  $s_k$  is the sink/source in phase- $k$ . Mass transfer from gas phase to liquid

**Table 4** Apparent diffusion coefficients for helium gas under different temperatures

Temperature (°C)	Apparent diffusion coefficient ( $D_a, \times 10^{-10} \text{ m}^2/\text{s}$ )
20	1.22
40	1.58
60	2.68

phase following Henry's law is captured by the  $s_k$ . For gases, such as helium gas, ideal gas law can be applied:

$$u_g = c_g RT \quad (7)$$

where  $R$  is the universal gas constant ( $8.314 \text{ J/mol/K}$ ) and  $T$  is the temperature (K).

Literature reveals that temperature can also affect the gas transport in initially saturated bentonite by different mechanisms, including its impacts on contact angle, surface tension, pore size and volume change. Since the diffusion and solubility-controlled (DSC) flow concept was used to simulate gas transport in initially saturated bentonite, change of contact angle or surface tension was not considered in this work. Meanwhile, Ye et al. [41] reported that temperature could have marginal effects on the pore structure of saturated bentonite, and consequently, volume change of the specimen due to temperature variation was neglected. Only the governing gas transport equations are presented here. The model equations are presented for two-phase gas–water flow in Cui et al. [4] to investigate gas transport processes in variably saturated porous media (e.g. evolution of the medium from partially saturated to fully saturated state, and vice versa) which is of particular interest, especially, for the scenarios where the gas pressure is large enough to induce pressure driven two-phase flow in the media. The theoretical background and numerical

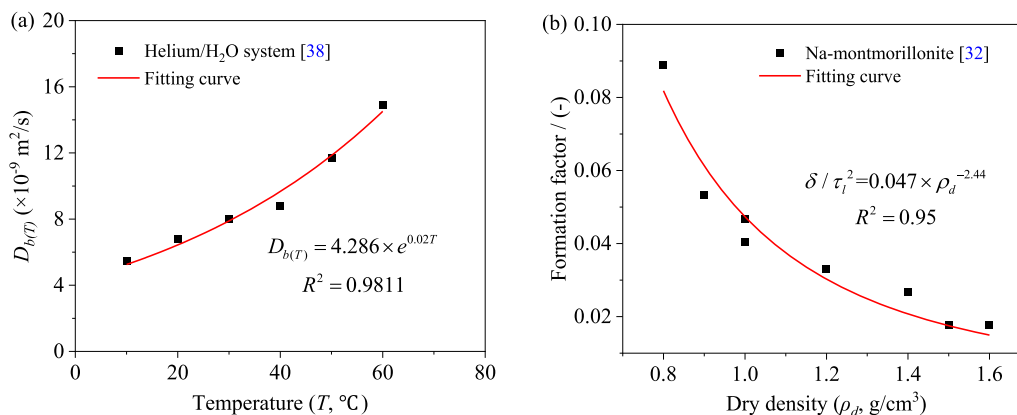


**Fig. 5** **a** Temperature variations in  $D_{b(T)}$  and **b** variations of dry density in formation factor,  $\delta/\tau_l^2$

formulation of the model are discussed comprehensively in Masum [25] and Vardon et al. [34].

### 3.4 Simulation set-ups

The test specimens were compacted to 10.21 mm height and 50.15 mm diameter cylinders. A 2D model domain of similar dimensions is created and discretized with equally spaced 4-noded quadrilaterals. The initial and boundary conditions of the fully saturated domain are presented in Table 5 and the parameters in Table 6.

## 4 Results and discussion

### 4.1 Evolution of gas pressure

Figures 6, 7 and 8 present a semi-logarithmic plot of the experimental and numerical results of gas pressures in both the injection compartment ( $P_1$ ) and receiving compartment ( $P_2$ ) versus time at different temperatures. Note that two different flow regimes can be classified in the experimental results of gas pressures as shown in Figs. 6, 7 and 8. For initial gas injection pressures lower than 4.11 MPa at 20 °C, 3.64 MPa at 40 °C and 2.63 MPa at 60 °C, flow regimes are similar to those presented in Figs. 6a, 7a and

**Table 5** Initial and boundary conditions used to simulate the gas breakthrough tests

Initial Conditions	Boundary conditions		Controlling temperature (°C)
	Injection boundary, $P_1$	Specimens	
$u_l = 0.0$ Pa	$u_g = 2.31$ MPa	1	20
$u_g = 0.0$ Pa	$u_g = 3.12$ MPa	2	20
$c_g = 0.0$ mol/ $m^3$	$u_g = 3.66$ MPa	3	20
$c_l = 0.0$ mol/ L	$u_g = 4.11$ MPa	4	20
	$u_g = 4.31$ MPa	5	20
	$u_g = 1.25$ MPa	6	40
	$u_g = 2.31$ MPa		
	$u_g = 3.15$ MPa		
	$u_g = 3.64$ MPa	7	40
		8	40
	$u_g = 3.94$ MPa	9	40
		10	40
	$u_g = 1.25$ MPa	11	60
	$u_g = 2.31$ MPa	12	60
	$u_g = 2.63$ MPa	13	60
	$u_g = 2.92$ MPa	14	60

**Table 6** Simulation parameters

Parameters	Values	Comments
Porosity, $n$	0.436	$\rho_d = 1.5$ g/ $cm^3$
Universal gas constant, $R$	8.314 J/mol/K	
Reference temperature, $T$	293.15 K 313.15 K 333.15 K	
Henry's constant, $K_H$	2580 L·atm/mol 2585 L·atm/mol 2437 L·atm/mol	293.15 K 313.15 K 333.15 K
Apparent diffusion coefficient of helium gas, $D_a$	$1.22 \times 10^{-10}$ m <sup>2</sup> /s $1.58 \times 10^{-10}$ m <sup>2</sup> /s $2.68 \times 10^{-10}$ m <sup>2</sup> /s	293.15 K 313.15 K 333.15 K
Formation factor, $\delta/\tau_1^2$	0.018	$\rho_d = 1.5$ g/ $cm^3$

8a, respectively. The  $P_2$  pressure increased slowly without observing any breakthrough. Once the initial pressure was increased to 4.31 MPa at 20 °C, 3.94 MPa at 40 °C and 2.92 MPa at 60 °C, flow regimes changed, respectively, e.g. Figs. 6b, 7b and 8b, and gas breakthrough was observed.

As shown in Fig. 6a, at the initial stage of gas injection, gas entered slowly into the porewater from the  $P_1$  boundary. During this period, helium firstly dissolved in the porewater and then diffused towards the  $P_2$  boundary, and finally released through the  $P_2$  boundary at the receiving compartment. This was evidenced by the gas pressure in the receiving compartment, where an approximate increase of 20 kPa was observed after 588 h of gas injection (Fig. 6a). This process was successfully captured by the proposed diffusion and solubility-controlled processes. The simulated  $P_2$  pressure was slightly lower than that of the observed during the initial 100 h of gas injection. Cui et al. [4] reported that some residual water in the tubing and the stainless-steel porous disc of the apparatus were dispelled to the receiving compartment under the applied initial gas pressure gradient. Consequently, the free gas-filled volume of the receiving compartment decreases, resulting in the measured gas pressure being higher than the model predicted values. With continuous diffusion, the simulated gas pressure gradually evolved and follows the similar trend to the experimental curve until the gas injection test was ceased after about 500 h, without observing gas

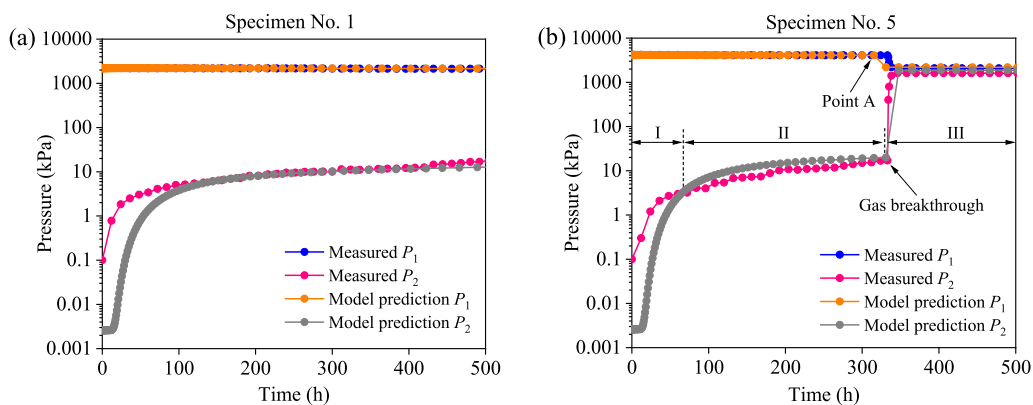


**Fig. 6** Evolution of gas pressures with time during gas injection tests at 20 °C under different initial pressure gradients

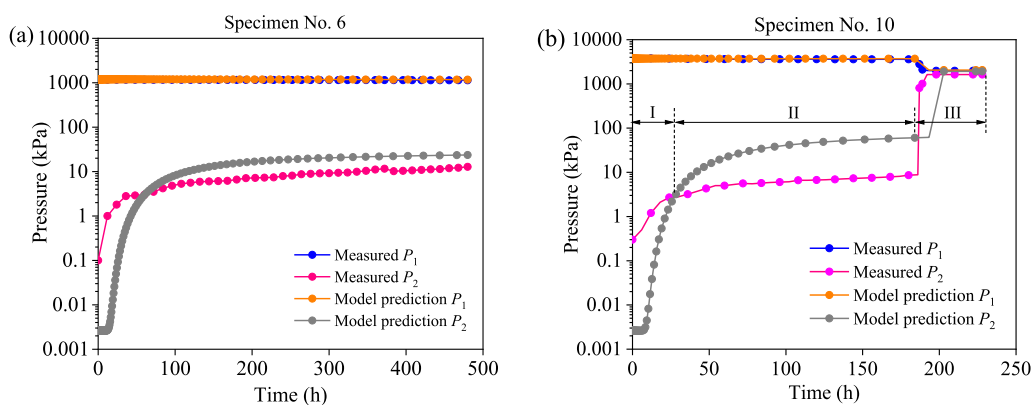


**Fig. 7** Evolution of gas pressures with time during gas injection tests at 40 °C under different initial pressure gradients

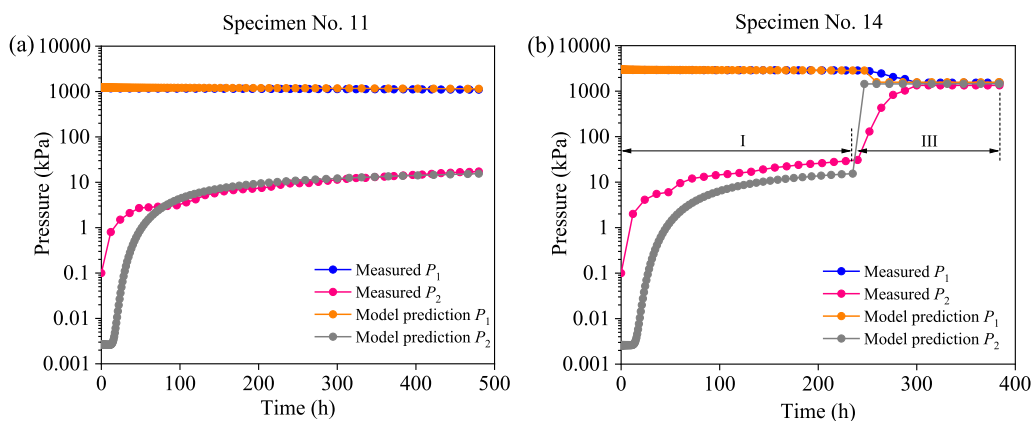


**Fig. 8** Evolution of gas pressures with time during gas injection tests at 60 °C under different initial pressure gradients

breakthrough. The specimens tested at 40 and 60 °C exhibit similar behaviour to that at 20 °C during both the experimental and the simulation studies. As shown in Figs. 7a and 8a, gas pressure in the receiving compartment increased to 12.8 and 17.3 kPa at the end of gas injection tests at temperatures 40 and 60 °C, respectively. However, for specimen No. 6 (Fig. 7a), the simulated gas pressure did not increase as quickly as the experimental value but

exhibited an overestimation of gas pressure after about 60 h of gas injection. Explanation to this discrepancy could be related to the possible overestimation of the effective transport-through porosity ( $\eta$ ) in Eq. (4). In this study,  $\eta$  was considered to be same as the as-prepared porosity of the specimen for all the cases in this study. In reality,  $\eta$  is perhaps smaller than  $n$  because of dead or unconnected pores in bentonite, which do not contribute to the overall



solute transport process [22]. No gas breakthrough was observed in these results, indicating that the porewater in the entire domain or in the accessible diffusion channels remains under-saturated, i.e.  $\Omega < 1.0$ , with respect to the dissolved helium gas and the solubility limit is not exceeded,  $c_l^{He} < c_{l,max}^{He}$ .

Figure 6b presents the gas injection results for bentonite tested at 20 °C with an obvious observation of gas breakthrough. The black lines in Fig. 6b represent the three events of simulation results, which separate the test into three stages, i.e. stage I, II and III. Results in stage I and stage II indicate that, following an instantaneous application of 4.31 MPa of helium, the simulated  $P_2$  pressure increased slowly from 0.1 to 17.1 kPa during 333 h of gas injection. The simulation results also exhibited an underestimation of the  $P_2$  values in the initial 60 h of gas injection (stage I) while a slight overestimation was observed in stage II, which is similar to those observed in Figs. 6a, 7a and 8a. Specifically, the gas breakthrough phenomenon in stage III was also successfully captured by the simulation results, which is characterized by a sharp decline in the  $P_1$  pressure and a rapid increase of the  $P_2$  pressure at the 334th hour of gas injection. In this case, the porewater solution is either in equilibrium ( $\Omega = 1.0$ ) or oversaturated ( $\Omega > 1.0$ ) with the dissolved helium gas ( $c_l^{He} \geq c_{l,max}^{He}$ ), and the system has reached to a steady state, as presented in Fig. 4. It should be noted that the supersaturation phase represents the state when the entire system is fully gas saturated, i.e. the solubility limit of bentonite porewater has been exceeded (beyond the equilibrium of gas dissolution and exsolution) and no more gas can be dissolved into the bentonite pore water. That means the helium solubility limit has already been reached in the entire accessible porewater domain of the bentonite specimen and any dissolution of helium gas must require expulsion of equal amount from the porewater. At  $\Omega = 1.0$  the system is in spontaneous equilibrium. Meanwhile at  $\Omega > 1.0$  the expulsion of gas is forced by the dissolving gas front under a fully rigid boundary which leads to the gas breakthrough phenomenon. Following the gas breakthrough, both  $P_1$  and  $P_2$  pressure curves converged rapidly and approached to the residual capillary pressure of 0.38 MPa (also denoted as “snap-off” pressure). Similar behaviour was observed from the specimen tested at temperatures 40 and 60 °C with the initial injection pressures of 3.94 and 2.92 MPa. Therefore, the DSC flow concept can be applied to satisfactorily capture the gas breakthrough events observed in Figs. 7b and 8b, respectively. The analyses reveal that the diffusion and solubility-controlled flow can adequately describe gas transport and breakthrough behaviours in rigidly confined, compacted

GMZ bentonite specimens submitted to variable temperature conditions.

## 4.2 Effects of gas pressure and temperature on dissolution and diffusion processes

Temperature effects on gas dissolution and diffusion processes could be evaluated by the diffusive flux across the saturated bentonite specimen, which is reflected by the rate of pressure increase in the closed gas receiving compartment. Therefore, evolution of  $P_2$  pressure with time tested at different temperatures is shown in Figs. 9, 10 and 11. Results in Figs. 9, 10 and 11 show that the  $P_2$  pressure increased almost linearly with time and the increase rate is dependent on the initial pressure difference. Meanwhile, for specimens tested at 20 °C, the pressure curve for specimen No. 1 with  $P_1 = 1.25$  MPa showed obvious fluctuations. However, this fluctuation phenomenon of the  $P_2$ -time curve was gradually diminished (with  $R^2$  closer to 1) as the  $P_1$  pressure was further increased (specimen No. 4), indicating the gas migration could become more stable under higher pressure levels. Furthermore, results in Figs. 9, 10 and 11 show that, for bentonite specimens tested at different temperatures, the  $P_2$ -time curves increased more rapidly at a higher initial gas pressure difference. Explanations to this phenomenon could be that, although the diffusion coefficient is fixed at a given temperature, the solubility of helium gas in water showed a linear relationship with pressure as shown in Fig. 3, which will induce that the diffusive gas flux increased as the initial gas pressure difference increased.

Figure 12 presents the gas flux (increase rate of  $P_2$  pressure, kPa/h) for bentonite tested at temperatures of 20, 40 and 60 °C. Please note that for bentonite specimens with an observation of gas breakthrough, the increasing rate of  $P_2$  pressure is defined as the slope of  $P_2$ -time curve before gas breakthrough. The relationship between the gas flux and the initial gas pressure difference ( $\Delta P = P_1 - P_2$ , kPa) for bentonite specimens tested at 20, 40 and 60 °C could be, respectively, fitted as,

$$\frac{dP_2}{dt} = 0.054 \cdot \exp(\Delta P/7422) - 0.047, R^2 = 0.905 \quad (8)$$

$$\frac{dP_2}{dt} = 0.006 \cdot \exp(\Delta P/1325) + 0.008, R^2 = 0.988 \quad (9)$$

$$\frac{dP_2}{dt} = 0.003 \cdot \exp(\Delta P/812) + 0.024, R^2 = 0.988 \quad (10)$$

Results in Fig. 12 showed that the gas flux increased almost exponentially with the initial pressure difference, i.e. the increasing rate of  $P_2$  was gradually augmented with the increase of initial pressure difference. At a same pressure difference, gas flux at temperature 60 °C was

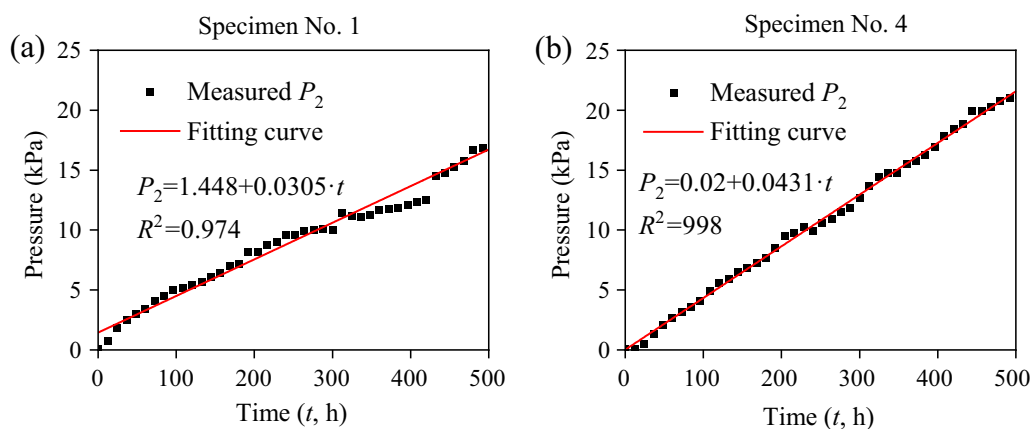


**Fig. 9** Evolution of pressure in the receiving compartment with time at 20 °C under different injection pressures

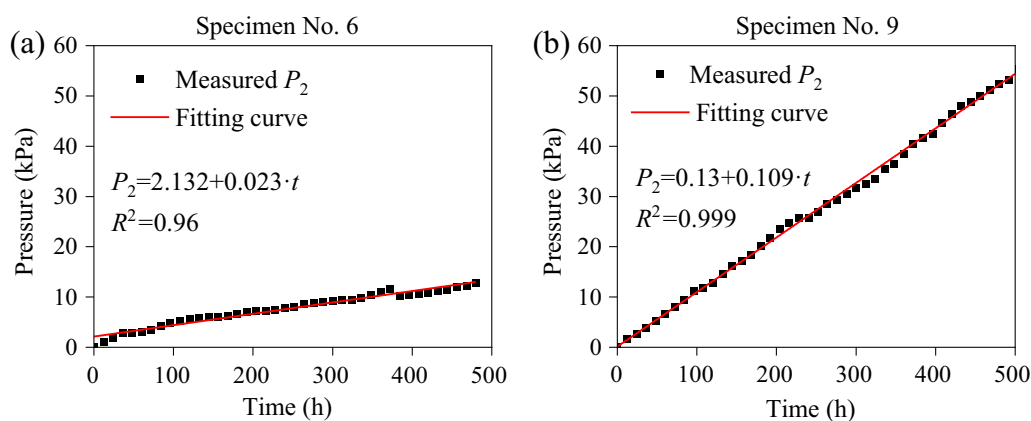


**Fig. 10** Evolution of pressure in the receiving compartment with time at 40 °C under different injection pressures

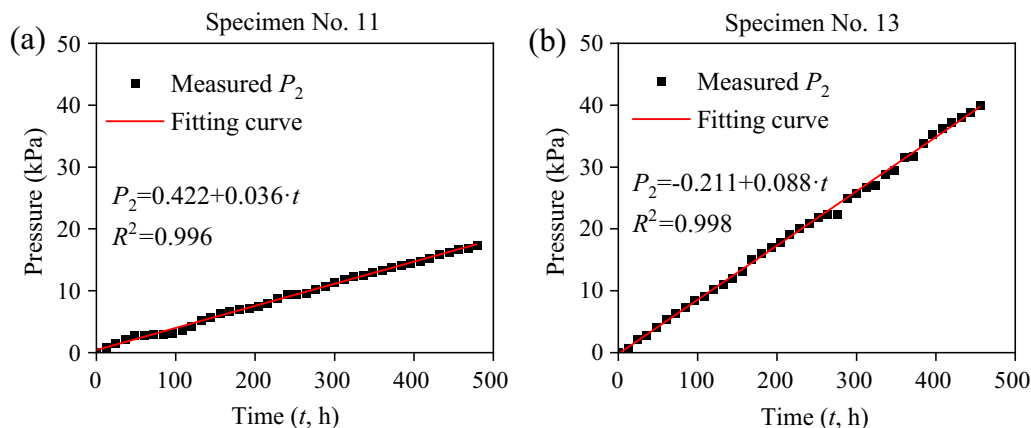


**Fig. 11** Evolution of pressure in the receiving compartment with time at 60 °C under different injection pressures

significantly higher than those at 20 and 40 °C. In fact, in water-saturated bentonites, as mentioned above, gas firstly dissolve in the porewater and the dissolved helium gas then diffuse through the porewater towards the receiving compartment, due to the concentration gradient. However, the solubility limit of helium gas at 60 °C exceeds that at 20

and 40 °C, leading to an elevated gas concentration gradient across the bentonite specimen. Meanwhile, at 60 °C, the apparent diffusion coefficients of helium gas in bentonite are almost twice as high as those observed at 20 and 40 °C (Table 4), which will finally induce a larger gas flow rate at a higher temperature. Furthermore, due to the large

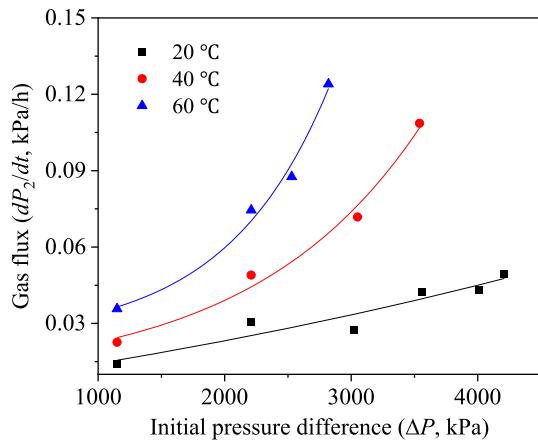


**Fig. 12** Relationship between increasing rate of  $P_2$  and the initial pressure difference at temperatures 20, 40 and 60 °C

specific surface area and negative charge of the montmorillonite, which is the dominant constituent of bentonite materials, large proportion of bentonite porewater remains strongly adsorbed onto the surface of clay minerals. Increasing temperature could induce transformation of adsorbed water at the surface of clay particles into free water and therefore an augment of the radius of flow pathways [11, 30]. This could also result in a larger effective transport-through porosity, and more porewater will be involved in the process of diffusion of the dissolved helium, thus leading to a more pronounced increase of gas migration rate at a higher temperature.

### 4.3 Temperature effects on gas breakthrough behaviour

According to the gas injection results of Cui et al. [6], gas breakthrough was observed after 334 h of gas injection at 20 °C under an initial injection pressure 4.31 MPa. Meanwhile, for specimens tested at 40 and 60 °C, gas breakthrough was recorded after 186 and 240 h of gas injection with the initial injection pressures of 3.94 and 2.92 MPa, respectively. It is clear that the breakthrough pressure decreased by approximately 32% with increasing the temperature from 20 to 60 °C (Fig. 13). This result was not fully investigated by Cui et al. [6], where a decrease of liquid surface tension at higher temperatures accompanied by easier water displacement through the saturated bentonite specimen was used to explain this phenomenon. However, the solubility aspects of bentonite porewater and its capacity to transfer the dissolved gases were neglected. Actually, Henry's law constant at 60 °C is lower than those at 20 and 40 °C (Table 3), which means that the amount of helium gas that could be dissolved in the porewater at 60 °C is higher than those at 20 and 40 °C under the same gas pressure level. Therefore, the gas injection pressure

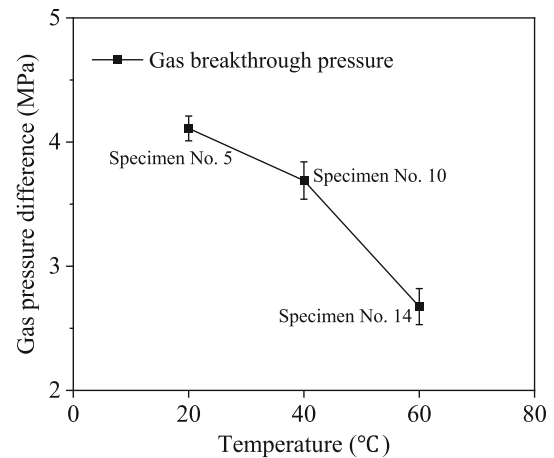


**Fig. 13** Gas breakthrough pressures required for gas breakthrough at different temperatures

required for porewater to be saturated with dissolved helium and exceed the solubility limit at 60 °C could be lower than that at 20 and 40 °C, which may eventually induce a lower breakthrough pressure for helium in saturated bentonite at higher temperatures.

The dissolved helium gas diffuses through the porewater towards the receiving compartment under the concentration gradient. Once the gases reach the interface between bentonite and receiving compartment, gases exit the specimens to the receiving compartment. Concentrations of dissolved helium in the  $P_1$  and  $P_2$  boundaries are proportional to the gas pressures in the injection and receiving compartments ( $P_1$  and  $P_2$ ), which could be estimated via Henry's law. As the gas injection tests proceeded, the concentration in the porewater increases with time along the depth of the specimen, i.e. from the injection compartment to the receiving compartment. However, the gas breakthrough does not occur until the concentration of dissolved helium ( $c_1^{He}$ ) exceeds the solubility limit ( $c_{l,max}^{He}$ ) in the entire domain. At elevated temperature, gas solubility increases which results into higher gas flux as shown in Fig. 12. As mentioned earlier that the porewater in saturated compacted bentonite exists as a gel-like substance which is denser than liquid water at ambient temperature. At elevated temperature, the viscosity as well as density of the gel is reduced, which accelerates diffusion of dissolved helium from  $P_1$  to the  $P_2$  boundary. This eventually leads to gas breakthrough occurring at lower pressures at higher temperatures. For specimens tested at 20 °C, if the injection pressures were below the breakthrough pressure, the helium concentration in the entire domain does not exceed the maximum solubility within the timescale of these experiments, which means the porewater is under-saturated with helium ( $\Omega < 1.0$ ) and more helium gas could be dissolved. As shown in Fig. 13, once the injection pressure

increased to 4.31 MPa, gas breakthrough was triggered because the entire domain in the specimen reached the solubility limit (value), which means the porewater is fully saturated with dissolved helium gas ( $\Omega \geq 1.0$ ).

## 5 Conclusion

In this study, the temperature effects on gas migration behaviour in saturated, compacted bentonite were investigated. Previously proposed diffusion and solubility-controlled (DSC) flow concept was tested to describe gas migration and breakthrough behaviour observed during laboratory experiments. Helium gas was injected into GMZ bentonite samples under rigidly confined boundary conditions at 20 °C, 40 °C and 60 °C. The main conclusions are drawn below.

- (1) The model predicted results showed good agreements with the experimental results, indicating that the DSC concept can adequately describe gas transport processes in saturated compacted bentonites that are subjected to rigid-boundary and elevated temperature conditions.
- (2) Observed fluctuations in gas pressures in the receiving compartment, at lower temperatures and lower injection pressures, suggest that helium gas dissolution and diffusion behaviours are sensitive to pressure and temperature. The behaviours in saturated, compacted bentonites become more stable with increase of gas injection pressure and ambient temperature.
- (3) Helium breakthrough pressure decreased by approximately 32% with increasing temperature (from 20 to 60 °C). This is because the amount of helium that can be dissolved in bentonite porewater at 60 °C is higher than that at 20 or 40 °C for the same gas pressure level. Therefore, the gas injection pressure required to saturate porewater with dissolved helium and exceed the solubility limit at 60 °C could be lower than that at 20 or 40 °C, which may eventually lead to a lower breakthrough pressure at higher temperatures.

Please note that the test specimens used in this study correspond to lower dry density bentonites. It is imperative to assess robustness and applicability of the diffusion and solubility-controlled gas transport and breakthrough mechanisms for higher dry density bentonite specimens. Further studies will be conducted in that regard.

**Acknowledgements** The authors are grateful to the National Natural Science Foundation of China (42202304) and the China Postdoctoral Science Foundation (2022M722391) for their financial support. The

support from Flexible Integrated System (Flexis) project and the China Scholarship Council are also greatly acknowledged.

**Open Access** This article is licensed under a Creative Commons Attribution 4.0 International License, which permits use, sharing, adaptation, distribution and reproduction in any medium or format, as long as you give appropriate credit to the original author(s) and the source, provide a link to the Creative Commons licence, and indicate if changes were made. The images or other third party material in this article are included in the article's Creative Commons licence, unless indicated otherwise in a credit line to the material. If material is not included in the article's Creative Commons licence and your intended use is not permitted by statutory regulation or exceeds the permitted use, you will need to obtain permission directly from the copyright holder. To view a copy of this licence, visit <http://creativecommons.org/licenses/by/4.0/>.

## References

1. PF Boulin P Bretonnier V Vassil A Samouillet M Fleury JM Lombard 2013 Sealing efficiency of caprocks: experimental investigation of entry pressure measurement methods *Mar Pet Geol* 48 20 30 <https://doi.org/10.1016/j.marpetgeo.2013.07.010>
2. P Braun S Ghabezloo P Delage J Sulem N Conil 2021 Thermo-poro-elastic behaviour of a transversely isotropic shale: thermal expansion and pressurization *Rock Mech Rock Eng* 54 1 359 375 <https://doi.org/10.1007/s00603-020-02269-y>
3. A Burghignoli A Desideri S Miliziano 2000 A laboratory study on the thermomechanical behaviour of clayey soils *Can Geotech J* 37 4 764 780 <https://doi.org/10.1139/t00-010>
4. Cui LY, Masum SA, Ye WM, Thomas HR (2021b) Investigation on gas migration behaviours in saturated compacted bentonite under rigid boundary conditions. *Acta Geotech.* <https://doi.org/10.1007/s11440-021-01424-1>
5. YJ Cui AM Tang C Loiseau P Delage 2008 Determining the unsaturated hydraulic conductivity of a compacted sand-bentonite mixture under constant-volume and free-swell conditions *Phys Chem Earth Parts A/B/C* 33 S462 S471 <https://doi.org/10.1016/j.pce.2008.10.017>
6. LY Cui WM Ye Q Wang YG Chen B Chen YJ Cui 2019 Investigation on gas migration in saturated bentonite using the residual capillary pressure technique with consideration of temperature *Process Saf Environ Prot* 125 269 278 <https://doi.org/10.1016/j.psep.2019.03.036>
7. LY Cui WM Ye Q Wang YG Chen B Chen YJ Cui 2020 Insights into determination of gas breakthrough in saturated compacted Gaomiaozhi bentonite *J Mater Civ Eng* 32 7 04020190 [https://doi.org/10.1061/\(ASCE\)MT.1943-5533.0003206](https://doi.org/10.1061/(ASCE)MT.1943-5533.0003206)
8. LY Cui WM Ye Q Wang YG Chen B Chen YJ Cui 2021 Insights into gas migration behavior in saturated GMZ bentonite under flexible constraint conditions *Constr Build Mater* 287 123070 <https://doi.org/10.1016/j.conbuildmat.2021.123070>
9. P Delage N Sultan YJ Cui 2000 On the thermal consolidation of Boom clay *Can Geotech J* 37 2 343 354 <https://doi.org/10.1139/t99-105>
10. I Deniau I Devol-Brown S Derenne F Behar C Largeau 2008 Comparison of the bulk geochemical features and thermal reactivity of kerogens from Mol (Boom Clay), Bure (Callovo-Oxfordian argillite) and Tournemire (Toarcian shales) underground research laboratories *Sci Total Environ* 389 2–3 475 485 <https://doi.org/10.1016/j.scitotenv.2007.09.013>

11. B Derjaguin V Karasev E Khromova 1992 Thermal expansion of water in fine pores *Prog Surf Sci* 109 2 586 587 [https://doi.org/10.1016/0079-6816\(92\)90067-R](https://doi.org/10.1016/0079-6816(92)90067-R)
12. C Gallé 2000 Gas breakthrough pressure in compacted Fo–Ca clay and interfacial gas overpressure in waste disposal context *Appl Clay Sci* 17 1–2 85 97 [https://doi.org/10.1016/S0169-1317\(00\)00007-7](https://doi.org/10.1016/S0169-1317(00)00007-7)
13. J Graham KG Halayko H Hume T Kirkham M Gray D Oscarson 2002 A capillarity-advective model for gas break-through in clays *Eng Geol* 64 2–3 273 286 [https://doi.org/10.1016/S0013-7952\(01\)00106-5](https://doi.org/10.1016/S0013-7952(01)00106-5)
14. C Graham J Harrington R Cuss P Sellin 2012 Gas migration experiments in bentonite: implications for numerical modelling *Miner Mag* 76 8 3279 3292 <https://doi.org/10.1180/minmag.2012.076.8.41>
15. Grathwohl P (2012) Diffusion in natural porous media: contaminant transport, sorption/desorption and dissolution kinetics. Springer
16. JF Harrington de La Vaissie're R, Noy DJ, Cuss RJ, Talandier J, 2012 Gas flow in Callovo-Oxfordian claystone (COx): results from laboratory and field-scale measurements *Miner Mag* 76 8 3303 3318 <https://doi.org/10.1180/minmag.2012.076.8.43>
17. Harrington JF, Horseman ST (2003) Gas migration in KBS-3 buffer bentonite. British Geological Survey. Technical Report TR-03-02
18. JF Harrington CC Graham RJ Cuss S Norris 2017 Gas network development in a precompact bentonite experiment: Evidence of generation and evolution *Appl Clay Sci* 147 80 89 <https://doi.org/10.1016/j.clay.2017.07.005>
19. T Higashihara H Shibuya S Sato T Kozaki 2005 Activation energy for diffusion of helium in water-saturated, compacted Namontmorillonite *Eng Geol* 81 3 365 370 <https://doi.org/10.1016/j.enggeo.2005.06.017>
20. A Hildenbrand S Schlömer BM Krooss 2002 Gas breakthrough experiments on fine-grained sedimentary rocks *Geofluids* 2 1 3 23 <https://doi.org/10.1046/j.1468-8123.2002.00031.x>
21. Hume HB (1999) Gas breakthrough in compacted Avonlea bentonite. Dissertation, University of Manitoba
22. DA Lever M Bradbury S Hemingway 1985 The effect of dead-end porosity on rock-matrix diffusion *J Hydrol* 80 1–2 45 76 [https://doi.org/10.1016/0022-1694\(85\)90074-5](https://doi.org/10.1016/0022-1694(85)90074-5)
23. JF Liu F Skoczylas J Talandier 2015 Gas permeability of a compacted bentonite-sand mixture: coupled effects of water content, dry density, and confining pressure *Can Geotech J* 52 8 1159 1167 <https://doi.org/10.1139/cgj-2014-0371>
24. P Marschall S Horseman T Gimmi 2005 Characterisation of gas transport properties of the Opalinus Clay, a potential host rock formation for radioactive waste disposal *Oil Gas Sci Technol* 60 1 121 139 <https://doi.org/10.2516/ogst:2005008>
25. S Masum P Vardon HR Thomas Q Chen D Nicholson 2012 Multicomponent gas flow through compacted clay buffer in a higher activity radioactive waste geological disposal facility *Miner Mag* 76 8 3337 3344 <https://doi.org/10.1180/minmag.2012.076.8.46>
26. A Mon J Samper L Montenegro A Naves J Fernández 2017 Long-term non-isothermal reactive transport model of compacted bentonite, concrete and corrosion products in a HLW repository in clay *J Contam Hydrol* 197 1 16 <https://doi.org/10.1016/j.jconhyd.2016.12.006>
27. Pusch R (1980) Permeability of highly compacted bentonite (No. SKBF/KBS-TR-80-16). Svensk Kaernbraenslefoerserjning AB
28. Pusch R (1980) Water uptake, migration and swelling characteristics of unsaturated and saturated, highly compacted bentonite (No. SKBF/KBS-TR-80-11). Svensk Kaernbraenslefoerserjning AB
29. A Rezaeyan SA Tabatabaei-Nejad E Khodapanah M Kamari 2015 Parametric analysis of caprock integrity in relation with CO<sub>2</sub> geosequestration: capillary breakthrough pressure of caprock and gas effective permeability *Greenhouse Gases: Sci Technol* 5 6 714 731 <https://doi.org/10.1002/ghg.1516>
30. Romero E, Gens A, Lloret A (2001) Temperature effects on the hydraulic behaviour of an unsaturated clay. In: Unsaturated soil concepts and their application in geotechnical practice, pp 311–332
31. Romero E, Gens A, Lloret A (2001) Laboratory testing of unsaturated soils under simultaneous suction and temperature control. In: Proceedings of the 15th international conference on soil mechanics and geotechnical engineering, Istanbul, pp 619–622
32. S Sato T Otsuka Y Kuroda T Higashihara H Ohashi 2001 Diffusion of helium in water-saturated, compacted sodium montmorillonite *J Nucl Sci Technol* 38 7 577 580 <https://doi.org/10.1080/18811248.2001.9715069>
33. Sedighi M, Bennett D, Masum S, Thomas H, Johansson E (2014) Analysis of temperature data at the Olkiluoto (No. POSIVA-WR-13-58). Posiva Oy
34. PJ Vardon HR Thomas SA Masum Q Chen D Nicholson 2014 Simulation of repository gas migration in a bentonite buffer *Proc Inst Civ Eng-Eng Comput Mech* 167 1 13 22
35. Z Wen 2006 Physical property of China's buffer material for high-level radioactive waste repositories *Chin J Rock Mech Eng* 25 4 794 800 in Chinese
36. R Wiebe VL Gaddy 1935 The solubility of Helium in water at 0, 25, 50 and 75 °C and at pressures to 1000 atmospheres *J Am Chem Soc* 57 5 847 851 <https://doi.org/10.1021/ja01308a017>
37. E Wilhelm R Battino RJ Wilcock 1977 Low-pressure solubility of gases in liquid water *Chem Rev* 77 2 219 262 <https://doi.org/10.1021/cr60306a003>
38. DL Wise G Houghton 1966 The diffusion coefficients of ten slightly soluble gases in water at 10–60°C *Chem Eng Sci* 21 11 999 1010 [https://doi.org/10.1016/0009-2509\(66\)85096-0](https://doi.org/10.1016/0009-2509(66)85096-0)
39. J Wollenweber S Alles A Busch BM Krooss H Stanjek R Litke 2010 Experimental investigation of the CO<sub>2</sub> sealing efficiency of caprocks *Int J Greenh Gas Control* 4 2 231 241 <https://doi.org/10.1016/j.ijggc.2010.01.003>
40. L Xu WM Ye B Ye 2017 Gas breakthrough in saturated compacted GaoMiaoZi (GMZ) bentonite under rigid boundary conditions *Can Geotech J* 54 8 1139 1149 <https://doi.org/10.1139/cgj-2016-0220>
41. WM Ye M Wan B Chen Y Chen Y Cui J Wang 2013 Temperature effects on the swelling pressure and saturated hydraulic conductivity of the compacted GMZ01 bentonite *Environ Earth Sci* 68 1 281 288 <https://doi.org/10.1007/s12665-012-1738-4>
42. WM Ye L Xu B Chen YG Chen B Ye YJ Cui 2014 An approach based on two-phase flow phenomenon for modeling gas migration in saturated compacted bentonite *Eng Geol* 169 124 132 <https://doi.org/10.1016/j.enggeo.2013.12.001>
43. Zeng Z, Cui YJ, Talandier J (2021) Investigating the swelling pressure of highly compacted bentonite/sand mixtures under constant-volume conditions. *Acta Geotech.* <https://doi.org/10.1007/s11440-021-01352-0>
44. CL Zhang N Conil G Armand 2017 Thermal effects on clay rocks for deep disposal of high-level radioactive waste *J Rock Mech Geotech Eng* 9 3 463 478 <https://doi.org/10.1016/j.jrmge.2016.08.006>

**Publisher's Note** Springer Nature remains neutral with regard to jurisdictional claims in published maps and institutional affiliations.